Recombination and regeneration dynamics in FeNHC(ii)-sensitized solar cells

Edoardo Marchini, Mohamed Darari, Luca Lazzarin, Rita Boaretto, Roberto Argazzi, Carlo Alberto Bignozzi, Philippe Gros, Stefano Caramori

COMMUNICATION

Recombination and Regeneration Dynamics in FeNHC (II)-sensitized solar cells

Received 00th January 20xx,
Accepted 00th January 20xx

DOI: 10.1039/x0xx00000x

Edoardo Marchini,[a] Mohamed Darari,[c] Luca Lazzarin, [a] Rita Boaretto,[a] Roberto Argazzi, [b] Carlo Alberto Bignozzi,[a] Philippe C. Gros,[c,*] and Stefano Caramori [a,*]

Recombination and regeneration dynamics in Fe-NHC-sensitized DSSCs revealed incomplete injection and the detrimental role of photoinjected electrons recapture by the I_3^- form of the redox electrolyte on performance. Importantly, the use of additives in the electrolyte allowed to reach the best efficiency ever recorded for an iron-based DSSC.

Dye-sensitized solar cells (DSSCs) are popular photovoltaic devices because of their low cost and transparency.[1] Their principle is to harvest solar photons using a sensitizer, linked to a photoanode (coated with n-type TiO_2 semiconductor (SC)). Upon light excitation, the sensitizer promptly injects its electron into the SC. A redox mediator then regenerates the sensitizer's ground state and is in turn regenerated at the cathode thus completing the electric circuit. Ruthenium polypyridine complexes have long been considered as top sensitizers due to their ideal photophysical and redox properties,[2] reaching up to 11-14% conversion efficiency.[3] Despite all these impressive properties, ruthenium remains a scarce and expensive metal limiting the real-world industrial development. This has motivated the quest for alternative metals such as iron[4, 5]. Unfortunately, conventional Fe(II) polypyridyl complexes are characterized by an ultrafast (*ca.* 100 fs) deactivation of the MLCT manifold to metal-centered (MC) states.[6-9] Thus, the too short lived the excited state impedes injection into the SC conduction band. One of the most successful strategies employed to delay the deactivation is to increase the ligand field strength.[10-16] Significant advances have been recently reported by the use of Pyridyl-N-heterocyclic carbenes (NHC),[10, 13-16] resulting in notable improvement of ^{3}MLCT lifetimes up to 16 ps[13] for complex **C1** (inset Figure 1) combining σ-donating NHCs and π-accepting carboxylic groups to be covalently grafted to the TiO_2 surface. The first photovoltaic characterization of a Fe(II)-NHC complex, reported by some of us,[13, 17] revealed a weak power conversion efficiency (0.13%). In consideration of the excited state lifetime of **C1** (16 ps), we expect a sufficiently efficient injection into the SC, reported to occur ideally within the *fs* time scale.[18] Thus it was of crucial importance to identify the bottlenecks that still limit the efficiency of Fe(II) sensitized solar cells. Herein, we report the unprecedented investigation of recombination and regeneration dynamics involving **C1** (Inset Figure 1) adsorbed on either n-type TiO_2 or SnO_2 in the presence of I^-/I_3 as electrolyte as well as a new electrolyte allowing to reach ca. 1% PCE that is the best efficiency ever reported for an iron-sensitized DSSC.

Despite the presence of a single binding COOH group, FeNHC adsorbs strongly on TiO_2 leading to a well-defined MLCT absorption peak centred at 500 nm resulting in a nearly quantitative light harvesting at such wavelength (Figure S1). Similar harvesting efficiency is found with SnO_2 photoanodes (Figure S2). Since, as expected, **C1** is not emitting in fluid solution nor when loaded on solid thin films, its spectroscopic energy ($E_{0\text{-}0}$=2.26 eV) was evaluated from the onset of the MLCT band at 550 nm. The cyclic voltammetry (Figures S3-S4) carried out on the sensitized thin films, showed a quasi-reversible Fe(II)/(III) oxidation process ($E_{1/2}$ = 0.67 V vs SCE , ΔE_{peak} ≈ 100 mV) . Thus the first excited oxidation potential E^*_{ox} was found at -1.6 V vs SCE ensuring ample driving force (ca. -0.9 eV) for injection into TiO_2 whose flat band potential is typically reported[19] to lie at ca. -0.7 V vs SCE in organic electrolytes containing lithium salts. A screening of the effect of TiO_2 morphology was performed in order to select the optimal substrate for cell efficiency. Commercial transparent TiO_2 (Greatcell Solar 18NR-T) composed of ca. 20 nm nanoparticles (Figure S5) was used with (*BUL*) and without (*no BUL*) a blocking underlayer produced by spin coating a 0.3 M $Ti(OiPr)_4$ on top of FTO (Fluorine-Tin-Oxide, Figure S6). Similar configuration was used in the case of semi-opaque paste (Greatcell Solar 18NR-AO) where ca. 20 nm particles tasked with dye adsorption are mixed with large light scattering particles in the 100 nm range (Figure S7). SnO_2 electrodes were fabricated in a similar fashion, by exploiting a colloidal paste and a blocking underlayer made by spin coating $SnCl_2$. Different electrolytes were tested as well. The base formulation consisted in 0.1 M LiI, 0.1 M I_2, 0.6 M PMII (1-methyl-3-propyl-imidazolium iodide) and 0.05 M (*el1*) or 0.1 M

[a] Department of Chemical and Pharmaceutical Sciences, University of Ferrara, Via L.Borsari 46, 44121, Ferrara, Italy
[b] CNR-ISOF c/o Department of Chemical and Pharmaceutical Sciences, University of Ferrara, Via L.Borsari 46, 44121, Ferrara, Italy
[c] Université de Lorraine, CNRS, L2CM, F-54000 Nancy, France

† Footnotes relating to the title and/or authors should appear here.

Electronic Supplementary Information (ESI) available: [Experimental details on sensitization and cell fabrication, AFM imaging on TiO_2 photoanodes, additional electrochemical, photoelectrochemical and spectroscopic data]. See DOI: 10.1039/x0xx00000x

MgI_2 to which different additives including GuNCS (Guanidinium thiocyanate) (*el2*) (Table S1) and 4-tBuPy (*el3*) were added. A commercial high stability electrolyte (Dyesol HSE) was tested as well.

Current density vs Voltage (J-V) curves in Figure 1 show that a substantial improvement in photovoltaic performances (from 0.49 to 0.75 % efficiency (η)) with the use of the blocking underlayer (*BUL* electrodes), consistent with the increased shunt resistance which implies lower dark current flowing between -0.1 and -0.3 V. The use of *el2*, containing GuNCS and 0.1 M MgI_2 further enhances performances, with Jsc=3.3 mA/cm^2, Voc = 0.44 V, FF=0.63 and η≈1% (Table S1). This improvement was due to the presence of GuNCS which slightly increases fill factor and Voc, ostensibly helping to block recombination, while Mg^{2+}, being a cation with a high charge density may adsorb on the TiO_2 surface and induce a surface excess of I^-, speeding up dye regeneration. To the best of our knowledge this the best efficiency ever achieved in an iron sensitized DSSC. The use of opaque titania produces slightly better photocurrents, but marginally lower Voc and a similar efficiency was observed. The better photocurrent generated by the opaque paste is consistent with broader IPCE (Incident Photon to Current Conversion Efficiency) (Figure 2) thanks to the improved light scattering properties of 18NR-AO, but the conversion maximum around 50% was substantially identical to that observed with the transparent electrodes which were used for the spectroscopic investigation (vide infra). Thus the kinetic information extracted from transient spectroscopy can be safely extended to the case of opaque substrates.

Under comparable conditions (*BUL-el1*), a transparent N 719 sensitized reference cell produced a broader and higher IPCE spectrum (max. IPCE ≈80 %), Jsc ≈13 mA/cm^2 and η = 3.1% (Figures S8 and Table S1). The relatively small efficiency of the N 719 cell is due to lack of basic additives which enhance Voc and FF.

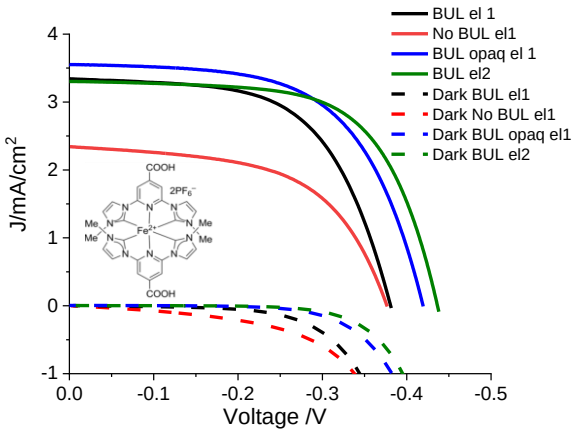

Figure 1. J-V curves of TiO_2 based **C1** sensitized solar cells under AM 1.5G illumination in the presence of I^-/I_3^- electrolyte. See main text and ESI for details on cell type and electrolyte formulation

This choice was motivated by the need of comparing **C1** and N 719 under identical electrolyte conditions. It was indeed reported by Housecroft et al.[20] that the presence of basic additives greatly depresses photocurrent in Fe(II) sensitized solar cells. We indeed confirmed the same trend here (Figure S9). J-Vs and IPCE with *el1* were also collected with SnO_2 based DSSCs where, despite the ca. 300 meV larger driving force for charge injection, we obtained a limiting photocurrent value ca. half that observed with *BUL-el1*, corresponding to an IPCE of ca. 25% and APCE (Absorbed Photon to Current Conversion Efficiency)≈30% (Figures S10). This suggested no thermodynamic limitation for charge injection into TiO_2 with respect to SnO_2 and the existence of fast recombination channels from SnO_2,[21] where the blocking underlayer had basically no effect on the resulting J-V characteristics (Figure S11). ‡

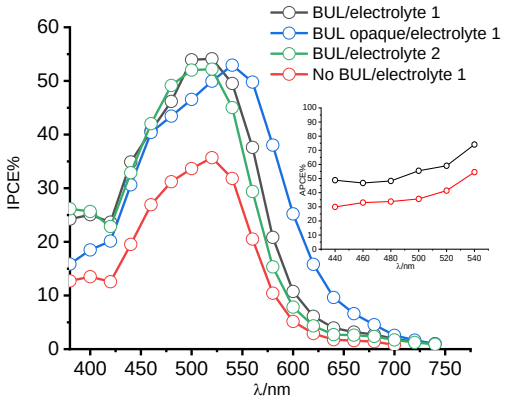

Figure 2. IPCE of TiO_2 based **C1** sensitized solar cells collected under short circuit in the presence of I^-/I_3^- based electrolytes. APCE spectra with B*UL/el1* (black) and *No BUL/el1* (red) are shown as inset

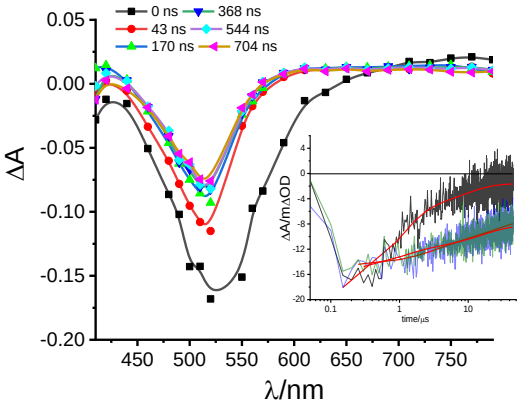

Figure 3. TAS of **C1** loaded on TiO_2 in contact with 0.1 M $LiClO_4$ in ACN upon 532 nm excitation. Inset: 500 nm recovery kinetics with (black) and without (blue (ACN/0.1 M $LiClO_4$, green (ACN/0.1M $LiClO_4$/0.2 M 4-TbuPy),) the presence of *el 2* deprived of the oxidized form of the mediator (I_2).

Considering the best IPCE recorded with *BUL* electrodes, we found a constant APCE=$\Phi_{inj}\times\eta_{coll}$ in the 55/60% range in agreement with the close to unity harvesting efficiency in the region corresponding to the maximum of the MLCT band. If the collection efficiency (η_{coll}) is unitary, this would set Φ_{inj} at a level of 50/60%. Under short circuit conditions, with *BUL*, considering the slow bielectronic reduction of I_3^- and the small monochromatic irradiance typical of quantum yield measurements, it is likely that η_{coll} will tend to unity, if the dye is regenerated efficiently by the redox couple.

To probe regeneration and recombination dynamics we performed transient absorption spectroscopy (TAS) in the

ns/ms time scale. TAS spectra at early delays after the laser pulse are shown in Figure 3. The photogeneration of the oxidized form of **C1** is practically instantaneous for our instrumental response (FWHM 7 ns), however a careful look at the TAS spectra at early delays evidences a spectral evolution that is substantially convolved with the laser pulse, resulting in the narrowing and the in minor blue shift of the MLCT bleaching associated to the disappearance of a weak absorption band rising for λ > 650 nm. Such dynamics is mostly evident by plotting the spectra during the first 4 ns after the laser pulse maximum (Figure S12), during which the FWHM of the bleaching band narrows from 91 to 73 nm while a blue shift of a few nm in the bleach minimum occurs. This spectral evolution could be assigned to the relaxation of a residual population of the lowest triplet state (T1). T1 could decay to the ground state either via non radiative pathways or by electron injection into TiO_2. The lower than unity Φ_{inj} extracted from APCE probably corroborates the first hypothesis. Nevertheless after ca. 40 ns such dynamics is complete, and no further change in the spectral shape is observed. This sets a lower limit for the injection rate constant of ca. 10^8 s^{-1}. The Fe(III) form of **C1** created upon laser excitation is thus characterized by the bleached MLCT band that mirrors the ground state absorption band and by a weak and featureless absorption extending to the red, probably originated by the absorption of LMCT states and of electrons photoinjected into TiO_2. In the absence of electron donor, the recovery of Fe(III) is power dependent and multiexponential, (Figure S13) stretching the time interval from a few μs to 0.1 s, owing to a distribution of electronic states in the semiconductor from which recombination occurs with different rates. At low laser energy (300 μJ/cm^2/pulse) the decay could be fitted with two components having approximately equal amplitudes, with time constants on the order of 2×10^{-3} s and 2×10^{-2} s respectively. At higher excitation fluences, a third component with a time constant in the scale of 10^{-4} s has to be added to account for the faster recombination as the number of electron/hole (Fe(III)) pairs in each TiO_2 nanoparticle increases. Nevertheless, even in the presence of the stronger excitation used in this work (ca. 18 mJ/cm^2/pulse), the decay of the charge separated state is less than 80% complete on a time scale of 0.1 s. By contrast, when iodide is present in overall 0.8 M concentration, 75 % of Fe(III) is regenerated on a time scale of 10 μs. A residual amplitude (ca 4 mΔOD) of the 500 nm bleaching however does not recover on this and on longer time scales. The TAS spectra in the presence of *el2* (omitting I_2) in the μs-ms range are shown in Figure 4.

The amplification of residual small ΔOD for t> 10μs evidenced in Figure 3 requires the application of 10 kOhm input impedance which increases the signal gain of our spectrometer by a factor of 200. The dynamics in the first 300 μs is thus substantially convolved with the laser pulse. Within this time window, we observe the fast recovery of the bleaching, accompanied by a red shift of ca. 40 nm. In the blue region, an absorption band rises, with a local maximum around 490 nm followed by a steep increase for λ< 450 nm. In the red, starting from 600 nm a flat absorption originated by photoinjected electrons increases (herein we have to assume that no LMCT states of Fe(III) are contributing, consistent with fast regeneration of Fe(II) observed at earlier delays). In the hundreds of μs to s range, such spectral features are then maintained with a slight reduction in their respective amplitudes due to charge recombination.

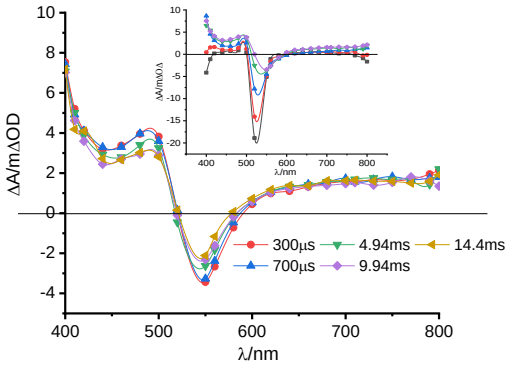

Figure 4. TAS (10 kOhm input impedance) of **C1** loaded on TiO_2 in contact with el2 deprived of I_2. The inset shows the evolution of the transient spectrum during the first 300 μs from excitation (0 μs (black), 20 μs (red), 60 μs (blue), 180 μs (green), 300 μs (purple))

We explain the initially fast bleach recovery as due to Fe(III) reduction by iodide, which results in the formation of triiodide, responsible for the absorption in the blue, particularly for the steep band rising for λ<420 nm.[22] Upon dye reduction, electrons are free to accumulate in the conduction band, where in the absence of oxidized form of the mediator (except the one which is locally photogenerated) they persist for several ms (Figure S21). The persistence and the shift of the bleach is not compatible with the fast electron donation evident in Figure 3, and is thus assigned to Stark effect,[22] resulting from electron accumulation in the mesoscopic semiconductor. The observed spectral changes are indeed consistent with spectro-electrochemical measurements (Figure S18) showing, upon negative polarization of the photoanode in the dark, a blue shift of the ground state absorption , which translates, in the difference spectra, in a relatively narrow bleach peaking around 530 nm accompanied by an absorption band peaking around 480 nm. This absorption feature agrees with the absorption band observed in Figure 4 within the same wavelength range. TAS in the presence of the complete *el2* (Figure S15) was partly disturbed by the strong absorption in the blue arising from the presence of I_3^-. It was nevertheless possible to confirm the presence of the Stark bleach, followed by the absorption of photoinjected electrons extending from 600 nm to 800 nm and beyond. The analysis of the recovery kinetics in such interval, compared to the previous case, where no I_3^- was initially present, allows to gain information about the dynamics of electron recapture by the oxidized mediator. In the absence of I_3^- the 750 nm absorption (Figure S21) is practically constant on a time scale of 20 ms, with only 6% of the initial ΔA amplitude recovering on such time scale. The small variation of the signal prevents the possibility of a reliable fitting. By contrast when 0.1 M I_2

was added to the electrolyte a decay with a time constant of 5.6 ms was observed (Figure S22), setting the apparent electron recapture rate constant by the redox couple in the order of 2 $\times 10^2$ s^{-1}. For comparison the N 719 electrode in the presence of the same *el2* electrolyte showed a time constant of ca. 18 ms (Figure S23), indicating a substantially slower electron recapture by the oxidized redox relay. This difference could be due to the different surface potential imparted to TiO_2 by adsorption of a positively charged dye in the case of **C1** (where the dissociation of one of the two carboxylic group may eventually reduce the complex charge from +2 to +1) (Figures S24-S27) and of a negative dye in the case of N 719. Cations present at the surface may eventually attract a local excess of iodide, instrumental to efficient regeneration, but also a surface excess of I_3^- which contributes to redox mediated recombination. The non-optimal shielding of the photoanode against recombination mediated by I_3^- may explain the strong effect of *BUL* in boosting cell performance in the case of **C1**. The comparison with transient data obtained with N719 also shows that at equivalent laser power the lifetime of Ru(III) (0.5 ms) (Figure S16) is considerably shorter than in the case of Fe(III) (14 ms). Nevertheless, this is not influencing the solar cell performance, since in both cases regeneration occurs in the µs time scale, leading to unit regeneration efficiency.

To conclude, this study has shown that despite the ps lifetime, **C1** gives rise to photoinduced injection into TiO_2 producing a long lived charge separated state ($e^-(TiO_2)$/Fe(III))surviving several milliseconds in an electrochemically inert electrolyte. Similar dynamics was found in the case of SnO_2, where, however recombination was faster and performances were generally lower than with TiO_2. Fe(III) could intercept iodide with unitary efficiency a feature which leads, when the photoanode is properly passivated, to the estimation, from APCE, of a quantum injection efficiency close to 50%.

This study points out some crucial factors affecting the performance of **C1**-sensitized DSSCs: i) The nature of the electrolyte and its additives GuNCS and MgI_2 by the way leading to the best performance obtained so far. ii) The recombination of photoinjected electrons with I_3^- due to positive surface potential established upon dye adsorption and the non-optimal screening of the TiO_2 surface from the access of I_3^-. iii) incomplete injection, resulting from kinetic competition of charge transfer with excited state deactivation. In consideration of the excited state energetics, this may result from non-optimal electronic coupling, arising from the symmetric design of **C1.** Work is in progress to chemically design new FeNHC sensitizers matching these requirements to open the way to efficient iron-based solar devices.

Conflicts of interest

There are no conflicts to declare.

Acknowledgements

The L2CM thanks the French Agence Nationale de la Recherche for a grant (ANR-16-CE07-0013-02) and is grateful to S. Parant for preliminary DSSC measurements. E.M. thanks the Fondo Sociale europeo Programma Operativo (2014-2020) Regione Emilia Romagana for a grant.

Notes and references

‡ TAS carried out on FeNHC sensitized SnO_2 in the µs-ms time scale showed the presence of a recombination component with a time constant of 10^{-4} s which persisted also at 350 µJ/cm^2/pulse. In addition, by comparing with TiO_2 at a comparable excitation fluence and optical density of the sensitized film, the initial amplitude of the FeNHC/SnO_2 signal was reduced by a factor of ca.10, suggesting the presence of an even faster recombination channel at earlier delays (Figure S14).

1 B. E. Hardin, E. T. Hoke, P. B. Armstrong, J.-H. Yum, P. Comte, T. Torres, J. M. Fréchet, M. K. Nazeeruddin, M. Grätzel and M. D. McGehee, *Nature Photonics*, 2009, **3**, 406.
2 J. P. Sauvage, J. P. Collin, J. C. Chambron, S. Guillerez, C. Coudret, V. Balzani, F. Barigelletti, L. De Cola and L. Flamigni, *Chem. Rev.*, 1994, **94**, 993-1019.
3 M. K. Nazeeruddin, F. De Angelis, S. Fantacci, A. Selloni, G. Viscardi, P. Liska, S. Ito, B. Takeru and M. Grätzel, *J. Am. Chem. Soc.*, 2005, **127**, 16835-16847.
4 S. Ferrere and B. A. Gregg, *J. Am. Chem. Soc.*, 1998, **120**, 843-844.
5 S. Ferrere, *Chem. Mater.*, 2000, **12**, 1083-1089.
6 O. S. Wenger, *Chem. Eur. J.*, 2019, **25**, 6043-6052.
7 J. E. Monat and J. K. McCusker, *J. Am. Chem. Soc.*, 2000, **122**, 4092-4097.
8 W. Zhang, R. Alonso-Mori, U. Bergmann, C. Bressler, M. Chollet, A. Galler, W. Gawelda, R. G. Hadt, R. W. Hartsock and T. Kroll, *Nature*, 2014, **509**, 345.
9 G. Auböck and M. Chergui, Nature chemistry, 2015, 7, 629.
10 Y. Liu, T. Harlang, S. E. Canton, P. Chábera, K. Suárez-Alcántara, A. Fleckhaus, D. A. Vithanage, E. Göransson, A. Corani and R. Lomoth, *Chem. Commun.*, 2013, **49**, 6412-6414.
11 T. C. Harlang, Y. Liu, O. Gordivska, L. A. Fredin, C. S. Ponseca Jr, P. Huang, P. Chábera, K. S. Kjaer, H. Mateos and J. Uhlig, *Nature Chem.*, 2015, **7**, 883.
12 Y. Liu, K. S. Kjær, L. A. Fredin, P. Chabera, T. Harlang, S. E. Canton, S. Lidin, J. Zhang, R. Lomoth and K. E. Bergquist, *Chem. Eur. J.*, 2015, **21**, 3628-3639.
13 T. Duchanois, T. Etienne, C. Cebrián, L. Liu, A. Monari, M. Beley, X. Assfeld, S. Haacke and P. C. Gros, *Eur. J. Inorg. Chem.*, 2015, 2469-2477.
14 L. Liu, T. Duchanois, T. Etienne, A. Monari, M. Beley, X. Assfeld, S. Haacke and P. C. Gros, *Phys. Chem. Chem. Phys.*, 2016, **18**, 12550-12556.
15 K. Magra, E. Domenichini, A. Francés-Monerris, C. Cebrian, M. Beley, M. Darari, M. Pastore, A. Monari, X. Assfeld and S. Haacke, *Inorg. Chem.*, 2019, **58**, 5069-5081.
16 M. Darari, E. Domenicchini, A. F. Monerris, C. C. Ávila, K. Magra, M. Beley, M. Pastore, A. Monari, X. Assfeld and S. Haacke, *Dalton Trans.*, 2019, **48**, 10915-10926.
17 M. Pastore, T. Duchanois, L. Liu, A. Monari, X. Assfeld, S. Haacke and P. C. Gros, *Phys. Chem. Chem. Phys.*, 2016, **18**, 28069-28081.
18 Y. Tachibana, J. E. Moser, M. Grätzel, D. R. Klug and J. R. Durrant, *J. Phys. Chem.*, 1996, **100**, 20056-20062.
19 Z. H. Bakr, Q. Wali, J. Ismail, N. K. Elumalai, A. Uddin and R. Jose, *Electrochimica Acta*, 2018, **263**, 524-532.

20 M. Karpacheva, C. E. Housecroft and E. C. Constable, *Beilstein J. Nanotechnol.*, 2018, **9**, 3069-3078.
21 A. N. Green, E. Palomares, S. A. Haque, J. M. Kroon and J. R. Durrant, *J. Phys. Chem. B*, 2005, **109**, 12525-12533.
22 S. Ardo, Y. Sun, A. Staniszewski, F. N. Castellano and G. J. Meyer, *J. Am. Chem. Soc.*, 2010, **132**, 6696-6709.